

Research paper

Drop impact onto a moving substrate: Aerodynamic rebound

Bastian Stumpf^a, Samaneh Abdi Qezeljah^a, Reda Kamal^{a,b}, Fabien Dezitter^c,
Alessandro Martuffo^d, Ilia V. Roisman^a, Jeanette Hussong^a*

^a Technische Universität Darmstadt, Institute of Fluid Mechanics and Aerodynamics, Darmstadt, 64289, Germany

^b Politecnico di Milano, Department of Aerospace Science and Technology, Milano, 20156, Italy

^c Airbus Helicopters S.A.S., Aéroport International Marseille Provence, Marignane, 13725, France

^d Airbus Helicopters, Aeromechanics & Performance, Marignane, 13725, France

ARTICLE INFO

Dataset link: <https://zenodo.org/doi/10.5281/zenodo.12684793>

Keywords:

Drop impact
Multiphase flow
Drop deposition and rebound
Boundary layer
Wetting and icing
Moving substrate

ABSTRACT

The dynamics of droplets approaching fast moving surfaces of high surface-tangential velocities is relevant to numerous technical applications, such as icing phenomena in aviation. Due to the substrate motion a boundary layer is formed which interacts with impacting droplets. In the present study, the transition from drop impact and splashing to boundary layer induced drop rebound is investigated for varying drop diameters, drop and plate velocity, as well as impact angles. It is found that this transition is strongly influenced by the degree of drop deformation that is induced by aerodynamic forces acting on the drop when it enters the boundary layer. Based on these considerations, a threshold model is obtained that describes the transition from splash to aerodynamic rebound. It is shown that the model is valid for a laminar and a turbulent boundary layer agreeing well with own and existing experimental data.

1. Introduction

The interaction of a drop with a planar surface that exhibits a fast motion tangential to its interface is relevant to numerous technical applications. One example is icing in aviation caused by small super-cooled drops in the atmosphere that impact onto the aircraft surface or onto rotating helicopter blades (Cao and Chen, 2010; Cao et al., 2018). Another example is droplet based cooling of fast rotating components, such as rotor windings in electric machines. In electrical machines, the interaction of the drop with the moving surface needs to be fully understood to be able to reliably predict the cooling heat flux (Lim and Kim, 2014; Liu et al., 2019). For this, it is of particular interest to know whether the droplets are in direct contact with the substrate and if so, what the impact outcome will be. For the icing, the resulting ice layer changes the aerodynamic properties of the aircraft, which leads to decreased efficiency and might lead to hazardous flight conditions (Lee et al., 1984; Kind et al., 1998; Cao et al., 2015; Yamazaki et al., 2021). Also, the ice accretion rate depends, among other phenomena, on the impact outcome. Generally, a drop impact can be subdivided into drop splash, deposition, or rebound. For reliable modeling of technically relevant processes, it is important to determine the deposited mass ratio and the parameters of the secondary spray formed by rebound and splash since this secondary spray could again impact onto surfaces.

The impact of drops onto stationary wetted and dry surfaces has been studied extensively (Yarin, 2006; Moreira et al., 2010; Josserand

and Thoroddsen, 2016; Yarin et al., 2017). The outcome of drop impact, it is bouncing (Sprittles, 2024), deposition and splash (Tropea and Marengo, 1999) is mainly determined by the impact parameters, the drop velocity $U_{d,n}$ normal to the substrate, and the drop diameter D and the material properties of the liquid, including the kinematic viscosity ν_{drop} , the density ρ_{drop} and the surface tension of the drop σ_{drop} . Correspondingly, the outcome is governed by the Reynolds number and Weber number, $\text{Re} = U_{d,n} D_{\text{drop}} / \nu_{\text{drop}}$ and $\text{We} = \rho_{\text{drop}} U_{d,n}^2 D_{\text{drop}} / \sigma_{\text{drop}}$, respectively. If the drop impacts onto a wetted substrate also the dimensionless film thickness, scaled by the drop diameter D , becomes an influencing parameter. Wall-normal drop impact onto a stationary and planar surface leads to a radially expanding flow in a thin lamella. The outcome is defined by the interaction of this flow with the outer wall film. If the inertial effects are dominant in comparison with the viscous and capillary forces, this interaction leads to the emergence of a corona-like liquid jet (Yarin and Weiss, 1995; Roisman and Tropea, 2002). The corona splash is then caused by the instability of the Taylor rim (Taylor, 1959; Roisman, 2010; Agbaglah et al., 2013; Wang and Bourouiba, 2021).

Drop impact onto a solid dry wall is influenced also by the conditions at the substrate surface, its morphology, and wetting properties (Mundo et al., 1995; Riboux and Gordillo, 2014; Roisman et al., 2015; Josserand and Thoroddsen, 2016). The evolution of the drop

* Corresponding author.

E-mail address: hussong@sla.tu-darmstadt.de (J. Hussong).

diameter is determined by the dynamics of the Taylor rim formed at the edge of the spreading lamella (Roisman et al., 2002). However, the outcome of drop impact depends significantly on the aerodynamic effects in the surrounding gas. It is known that the conditions leading to corona emergence and thus to the corona splash are influenced by the properties of the surrounding gas (Xu et al., 2005). Recently, the main mechanisms of the corona emergence associated with the dynamics of the gas flow in a spreading wedge has been considered and explained (Riboux and Gordillo, 2014).

Drop bouncing from a dry or even liquid surfaces occurs for impacts with relatively low Weber number, $We \sim \mathcal{O}(1)$. It is attributed to a very thin air layer between the substrate and the drop (de Ruiter et al., 2014). For the drop impact onto moving substrates (Mundo et al., 1995) showed that for the splash deposition limit only the normal component of the drop impact velocity is relevant if the tangential substrate velocity is smaller or comparable with the drop impact velocity. Most studies that investigated the interaction of a drop with a moving substrate focused on the hydrodynamics of spreading on wetting and non-wetting substrates (Almohammadi and Amirfazli, 2017; Moghtadernejad et al., 2021). Only a few studies investigated parameter ranges where the inertia of the gas boundary layer is sufficiently high to play a significant role in the drop dynamics. A complete aerodynamic rebound of droplets due to the airflow in the boundary layer was first observed and analyzed in Povarov et al. (1976). In this study, the threshold velocity U_{plate}^* of the substrate, corresponding to the inception of the drop rebound, is related to the thickness δ of the viscous boundary layer in the gas flow.

$$U_{plate}^* \sim U_{d,n} \sqrt{\frac{\rho_{drop}}{\rho_{gas}} \frac{D_{drop}}{\delta}}. \quad (1)$$

The same relation was confirmed by Gauthier et al. (2016, 2018) for laminar boundary layers.

In the present study, we show that the threshold velocity (1) at which droplet rebound can be observed is valid for both laminar and turbulent boundary layers. However, the coefficient of proportionality in (1) changes significantly. This means that not only the boundary layer thickness but also the velocity profile plays a significant role in the bouncing phenomenon.

2. Experimental setup

The experimental setup, schematically shown in Fig. 1(a), consists of the rotating plate, the drop generation system, and the imaging system. The plate is made of carbon fiber-reinforced plastic (CFRP) and has a radius of $R = 90$ mm. It is attached to a brushless DC motor that can accelerate the plate to an angular velocity of $\Omega \leq 17,000$ rpm (revolutions per minute). The velocity is controlled, monitored, and logged by an in-house LabView script. To capture the drop impact, a high-speed camera is used in the imaging system. Depending on the experiment the utilized models are either Photron SA-X2 or Phantom T3610. A high-speed LED (Constellation 120E) and a diffuser plate provide uniform background illumination, and the imaging system can reach frame rates of 100,000 fps. The spatial resolution in the experiments varies in the range of $9 \mu\text{m}$ to $15 \mu\text{m}$ per pixel.

The drop generator is a commercial mono-disperse drop chain generator from FMP Technology GmbH which will be referred to as FMP generator in the following. It generates a mono-disperse stream of droplets by inducing a Rayleigh–Plateau instability onto a liquid jet using a piezoelectric actuator (Brenn and Tropea, 1996). The droplet size can be varied in the range $80 \mu\text{m} \leq D \leq 500 \mu\text{m}$ by either changing the size of the outlet orifice of the FMP or by altering the excitation frequency. The radial coordinate of impact is 88 mm but can fluctuate approximately ± 1 mm. The absolute velocity of the droplet is set by controlling the pressure in the pressurized tank and can be varied in the range $5.5 \text{ m/s} \leq U_{d,abs} \leq 12 \text{ m/s}$. The velocity component $U_{d,n}$ of the drop normal to the plate can be altered by altering the impact

angle $10^\circ \leq \beta \leq 40^\circ$ of the droplet or $U_{d,abs}$. In Fig. 1(b) and Fig. 1(c), the geometry of the impact is illustrated. The normal and horizontal velocity components $U_{d,n}$ and $U_{d,h}$ can be obtained directly from the high-speed recordings, as will be explained below. A consequence of the inclined impact is that the droplet has a velocity component in circumferential direction $U_{d,\varphi} = U_{d,h} \cos \alpha$ where α is a constant offset angle of 7.1° , relative to the camera axis. To account for this the relative velocity in circumferential direction $U_{\varphi,rel}$ is considered the characteristic velocity which can be formed as

$$U_{\varphi,rel} = U_{\varphi,plate} - U_{d,\varphi}, \quad (2)$$

where $U_{\varphi,plate}$ represents the circumferential velocity of the plate. The plate Reynolds number, $Re_{aero} = r^2 \omega / \nu_a$, with ω being the angular velocity of the plate and ν_a the kinematic viscosity of air, varies in the range $2.5 \times 10^5 < Re_{aero} < 8.7 \times 10^5$. The lower limit is chosen to avoid the boundary layer's transitional regime, while the upper limit aligns with typical values for helicopter blades and aircraft wings. The corresponding plate velocity at the impact location is in the range $40 \text{ m/s} < U_{\varphi,plate} < 160 \text{ m/s}$.

At the upper end of this range, weak compressibility effects may be expected as the Mach number approaches approximately 0.5. Experimental results by Theodorsen and Regier (1944) for Mach numbers up to 0.62 indicate that the theoretical predictions by von Kármán (1946), which are based on the assumption of incompressibility, exhibit strong agreement with the experimental data for the moment coefficient, which in turn is derived from the boundary layer profile. Furthermore, the boundary layer profile shows a steep gradient near the wall, confining any compressibility effects to a small fluid region. Consequently, within the range investigated, compressibility effects are negligibly small and are therefore not considered in the present study.

Finally the boundary layer is fully turbulent, as the laminar-to-turbulent transition for the plate occurs in the range $1.8 \times 10^5 < Re_{aero} < 3.5 \times 10^5$, as shown in Shevchuk (2009).

2.1. Image processing

The experiments are analyzed in a custom MATLAB script, utilizing the MATLAB image processing toolbox, where the drop diameter as well as the horizontal and vertical velocity components of the drop before impact are measured. For this, first, a moving background subtraction with a delta of 5 frames followed by a binarization is performed. From the resulting binary images, individual objects i.e. droplets, their centroid, and diameter can be evaluated. A simple particle tracking algorithm based on the nearest neighbor principle is then used to recognize the droplets in consecutive frames and thus determine the trajectories. To make the evaluation more robust against false detection, only trajectories with objects that are recognized and allocated in 10 consecutive frames are considered. A median drop diameter is determined for each trajectory using images of the drop in multiple consecutive frames before impact. To address potential bias due to outliers, drop images with diameters that deviate more than two standard deviations from the mean are considered outliers and are excluded. Eventually, mean values of the diameter and the respective horizontal and vertical velocity components are formed using all trajectories in an experiment. Furthermore, cases in which the droplet diameter or the droplet impact velocity scatter by more than 20% are discarded from the evaluation. The mean relative standard deviation for all cases is $\bar{\sigma}_D = 4.49\%$ for the drop diameter, $\bar{\sigma}_{U_{d,n}} = 4.1\%$ in the normal direction and $\bar{\sigma}_{U_{\varphi,rel}} = 0.25\%$ for the relative plate velocity.

3. Results of drop impact and rebound

When consecutive, mono-disperse droplets interact with a rotating plate, various phenomena can be observed depending on the impact parameters. In Fig. 2, a time series of impacting droplets of constant diameter and velocity is shown at three different plate velocities. For

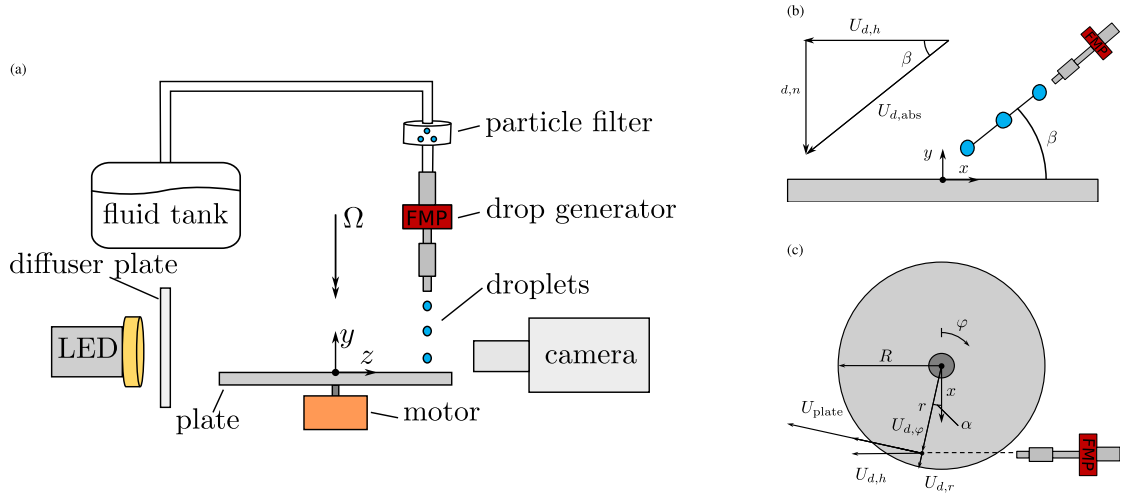


Fig. 1. Schematic representation of the experimental setup (a) side view (b) top view and (c) front view.

the lowest plate velocity, $U_{\varphi,rel} = 60 \text{ m/s}$ (see Fig. 2(a)) a strong interaction of the droplet with the plate can be observed. During the interaction, liquid adheres to the fast-moving plate and gets dragged along, while in parallel, ligaments form that atomize into secondary droplets and are carried away by the airflow in the boundary layer. The liquid that adheres to the plate will reach the impact location after one full revolution of the rotating plate where consecutive droplets may impact onto the now wetted surface. In this case, splashing is enhanced. Studies on single drop impact onto thin liquid films have shown that very thin films with dimensionless film thicknesses $\tilde{h} < 0.02$ enhance splashing significantly (Geppert, 2019; Zhu et al., 2021; Stumpf et al., 2023). In contrast, for the highest plate velocities, $U_{\varphi,rel} = 140 \text{ m/s}$ (see Fig. 2(c)) no splash and also no residual can be observed anymore, as droplets undergo a complete aerodynamic rebound, preventing drop-plate contact.

At medium plate velocities, $U_{\varphi,rel} = 80 \text{ m/s}$ (see Fig. 2(b)) splashing can only be observed occasionally and in a less pronounced form. Droplets partially rebound while it is evident in the enlarged section at $t = 0.1 \text{ ms}$ that a small amount of the droplet resides on the plate.

There are two reasons why the splash might only occur for some droplets:

- The turbulent character of the airflow leads to small fluctuations of the impact location in the radial direction that result in variations of the relative velocity at impact. The latter's are caused by the radial boundary layer of the disk and are within the depth of field of the camera leading to a possible error in the impact position of $\pm 2 \text{ mm}$. In consequence, when the plate velocity is close to the critical velocity for rebound, some of the drops will exceed it and only some drops will have contact with the plate.
- As depicted in Fig. 2(b) (see instant 0.01 ms), the interaction between the droplet and the plate results in the formation of small patches of residual liquid. At instants 0.10 ms and 0.11 ms it can be observed that such patches interact with a subsequent droplet after one revolution, resulting in a splash. It is evident that such patches potentially influence the outcome of subsequent drop impacts. However, these patches cannot be observed in the aerodynamic rebound regime.

Thus, for increasing plate velocity the transition from splash/contact to aerodynamic rebound is continuous. For the following analysis, three categories of interaction are defined. If the outcome of the impact results in a splash then the experiment will be classified as “splash/contact”. If splash can only be observed for some of the droplets then the experiment will be categorized as “transition”. If no splash can be observed throughout the experiment and the droplets are

completely repelled from the plate, we conclude that there is no more contact and thus no liquid residual on the plate. This regime is defined as “aerodynamic rebound”.

3.1. Observed impact outcomes

To characterize the outcome of the drop impact onto a rotating plate the normal impact velocity $U_{d,n}$ as well as the relative plate velocity $U_{\varphi,rel}$ and the drop diameter are systematically varied. In Fig. 3(a) the outcome of impact is shown for the relative tangential and normal impact velocity. It becomes apparent that for higher $U_{d,n}$ also higher $U_{\varphi,rel}$ are necessary to achieve aerodynamic rebound. A straight line could separate the aerodynamic rebound from the transition and splash in the plot. In Fig. 3(b) the outcomes are shown for a larger drop diameter of $D \approx 452 \mu\text{m}$. In comparison to the $D \approx 91.3 \mu\text{m}$ case for the larger drops, higher plate velocities are necessary to achieve an aerodynamic rebound. It becomes evident that the higher the inertia of the drop the higher also the inertia of the airflow needs to be to reflect the droplet from the plate.

In preceding studies (Povarov et al., 1976; Gauthier et al., 2018) threshold parameters, describing the onset of aerodynamic rebound and based on the relation of drop and plate inertia are formulated in (1) assuming a deceleration of the droplet throughout the boundary layer and possible trajectory deflection due to the aerodynamic drag. This assumption is examined in Fig. 4. In Fig. 4(a) the temporal evolution of the distance y of the center of mass of the drop to the plate and its velocity are exemplified for one experiment in the aerodynamic rebound regime. The instant $t = 0$ is defined as the time when the undeformed (spherical) drop with an undisturbed trajectory would touch the plate. In Fig. 4(b) the evolution of the corresponding velocity is shown. The estimated thickness of the turbulent boundary layer thickness in this case is $\delta_i \approx 4.5 \text{ mm}$. It can be seen that the center of mass of the droplet is not decelerated until it is in the close vicinity of the plate surface ($y \approx 100 \mu\text{m}$). This suggests that rather than the deceleration of the whole droplet, the deformation of the droplet is governing the rebound.

3.2. Boundary layer induced drop deformation: governing scales

The dynamics of a drop moving through an airflow is determined by a balance of the stresses in the airflow and in the deforming drop. The main aerodynamic stresses include

$$p_{\text{gas}} \sim \rho_{\text{gas}} U_{\text{gas}}^2, \quad (3)$$

$$p_{\text{unsteady}} \sim \rho_{\text{gas}} D_{\text{drop}} \frac{dU_{\text{gas}}}{dt} \sim \rho_{\text{gas}} D_{\text{drop}} \frac{\partial U_{\text{gas}}}{\partial z} U_{d,abs}, \quad (4)$$

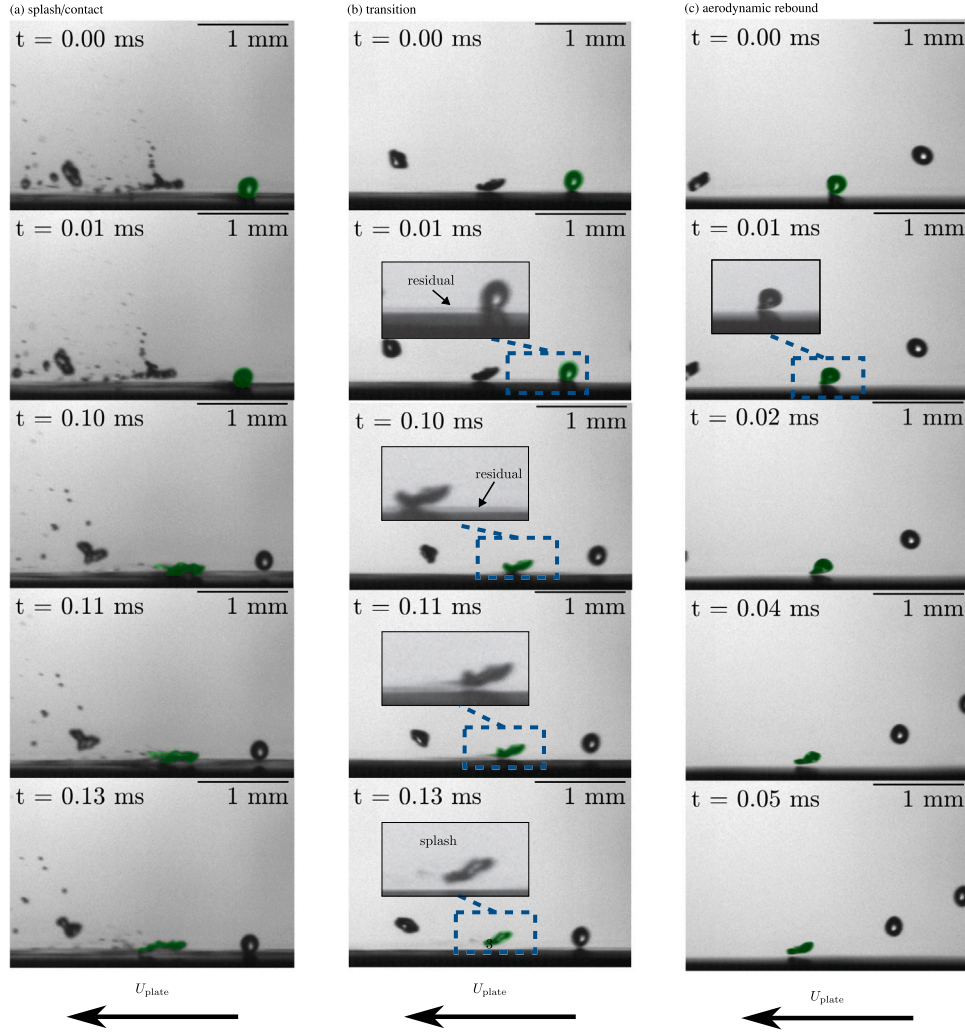


Fig. 2. Snapshots of a stream of monodisperse drops impacting on a plate at different plate velocities $U_{\phi,rel}$. The droplet of interest is highlighted with a green overlay. (a) splash occurring at $U_{\phi,rel} = 60$ m/s, (b) transition at $U_{\phi,rel} = 80$ m/s, (c) aerodynamic rebound at $U_{\phi,rel} = 140$ m/s. Impact parameters are $D \approx 230 \mu\text{m}$, $U_{d,n} \approx 2$ m/s, $\beta = 19^\circ$. The corresponding videos are available in the supplementary material. (For interpretation of the references to color in this figure legend, the reader is referred to the web version of this article.)

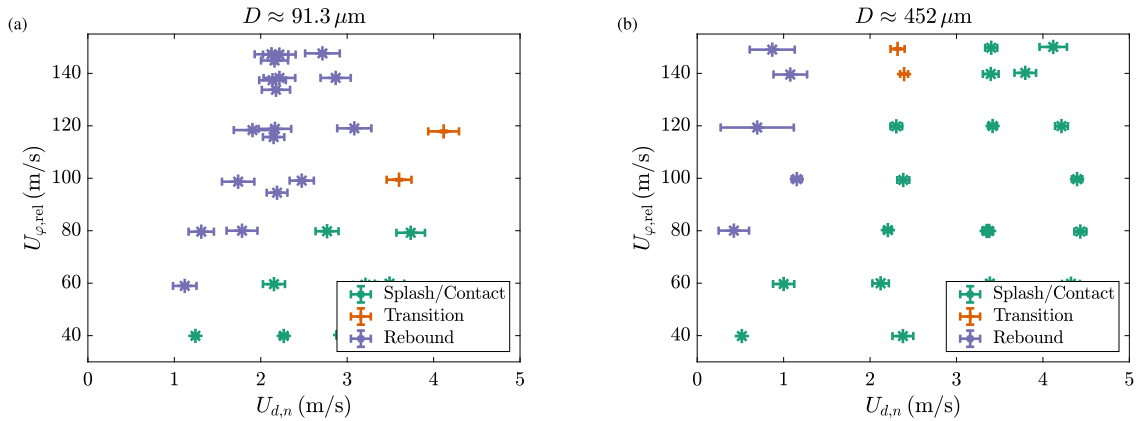


Fig. 3. Velocity maps showing the drop impact outcomes “splash”, “transition” and “rebound” for the plate velocity $U_{\phi,rel}$ and the normal drop impact velocity $U_{d,n}$ for (a) $D \approx 91.3 \mu\text{m}$, (b) $D \approx 452 \mu\text{m}$. The error bars show the root mean square error (RMSE) of the corresponding velocities of different drops in one experiment.

where U_{gas} is the relative gas velocity.

It can be shown that if the gas velocity is much higher than the drop velocity, $U_{\text{gas}} \gg U_{d,abs}$, the value of p_{unsteady} is negligibly small in comparison with p_{gas} . However, this is not the case when the thickness

of the boundary layer δ is much smaller than the initial diameter of the drop, D_{drop} .

The stresses in the drop are defined by the drop deformation velocity U_{def} . The pressure terms in the drop, arising from inertial effects

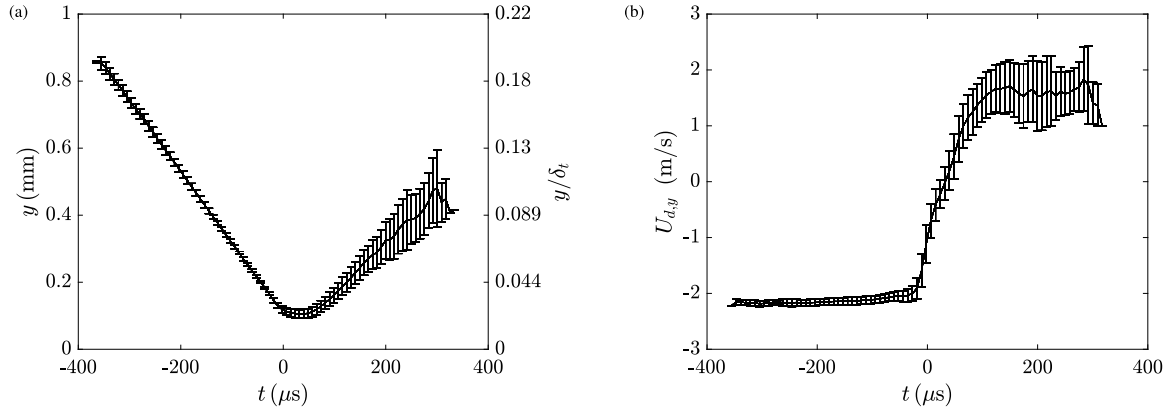


Fig. 4. Evaluation of the drop trajectory (a) normal distance to the plate as a function of time. (b) Velocity in normal direction as a function of time. Error bars are the RMSE between the trajectories in the experiment. Impact conditions: $U_{\varphi,rel} = 120$ m/s, $D = 218$ μ m, $U_{d,n} = 2.1$ m/s, $\beta = 19.25^\circ$.

due to the deformation flow, are

$$p_{drop} \sim \rho_{drop} U_{def}^2, \quad p_{drop, unsteady} \sim \rho_{drop} D_{drop} \frac{dU_{def}}{dt} \quad (5)$$

The drop deformation velocity outside the boundary layer is negligible, given that the aerodynamic pressure associated with the air relative velocity is considerably smaller than the capillary pressure of the drop. Upon entering the boundary layer, the relative gas velocity increases, resulting in the deformation of the drop. For the modeling of this stage of drop motion, it is sufficient to consider only the unsteady pressure term. The validity of this assumption will be examined later, once the deformation velocity has been determined. Consequently, the balance of pressure at the drop interface yields:

$$\rho_{gas} U_{gas}^2 = \rho_{drop} D_{drop} \frac{dU_{def}}{dt}. \quad (6)$$

The relative gas velocity profile in the boundary layer can be represented in the form

$$U_{gas} = U_{plate} f(\xi) - U_d \cos \beta, \quad \xi = \frac{z}{\delta}, \quad (7)$$

where $f(\xi)$ is a dimensionless function of the similarity variable ξ , and δ is the thickness of the boundary layer.

The solution of the differential Eq. (6) is obtained in terms of the variable ξ using the transformation of the variable $dt = \delta d\xi / U_{drop,n}$

$$U_{def}(\xi) = \frac{\delta \rho_{gas} U_{plate}^2}{D_{drop} \rho_{drop} U_{d,n}} \int_{\xi}^{\xi^*} [f(\xi) - k]^2 d\xi, \quad (8)$$

$$k = \frac{U_d \cos \beta}{U_{plate}}, \quad U_{d,n} = U_d \sin \beta, \quad (9)$$

where ξ^* is the dimensionless variable at which the relative gas velocity equals zero.

The aerodynamic rebound, defined as the onset of the upward movement of the droplet without contact with the wall, is driven by the aerodynamic forces experienced by the droplet within the boundary layer. These forces, in turn, cause the droplet to deform. The droplet rebound occurs if the deformation velocity at the wall ($\xi = 0$) is equal to the normal component of the droplet impact velocity $U_{d,n}$. This condition can now be written with the help of (8) in the form $B = B_{rebound}$ where

$$B = \frac{\delta \rho_{gas} U_{plate}^2}{D_{drop} \rho_{drop} U_{d,n}^2} \int_0^{\xi^*} [f(\xi) - k]^2 d\xi. \quad (10)$$

$B_{rebound}$ being an empirical constant of order of unity.

It is interesting that the scaling (10) has a form similar to that defined in (1), obtained in Gauthier et al. (2016, 2018) for laminar airflow from different considerations. In this study, the scaling is applied to the turbulent and laminar flows, generated by the rotating disk.

3.3. Solution for turbulent boundary layer

The regime of the flow around a rotating disk is determined by the aerodynamic Reynolds number Re_{aero} . As mentioned earlier, in this study the flow is turbulent for all the experimental conditions. An approximate solution for the turbulent boundary layer (Shevchuk and Khalatov, 1997) is chosen for the consideration of drop deformation. In this solution, the integral method is combined with the fitting of the existing experimental data from Cham and Head (1969), Itoh and Hasegawa (1994), Littell and Eaton (1994).

The profile of the thickness of the boundary layer is expressed as

$$\delta \approx 0.48 Re_{aero}^{-1/6} \quad (11)$$

In our experiments, the value of δ is of the order of 1 mm.

The azimuthal velocity component of the gas flow in the laboratory reference frame is assumed in the form $u_\varphi = f(\xi)$ with

$$f(\xi) \approx 1 - \xi^{1/9}, \quad \xi = \frac{z}{\delta}. \quad (12)$$

The power-law approximation was first proposed by von Kármán (1921) using an analogy with the turbulent flow in a round pipe and on a flat plate. While in the original work, the exponent is 1/7, from a comparison with the experimental result a better agreement is found with a value of 1/9, (Shevchuk, 2009). For more detailed information on the turbulent boundary layer approximation, the interested reader is referred to comprehensive reviews (Kobayashi, 1994; Crespo del Arco et al., 2005; Shevchuk, 2009; Lingwood and Henrik Alfredsson, 2015; Alfredsson et al., 2023).

Now, the coordinate ξ^* corresponding to the position at which the relative gas velocity equals zero is

$$\xi^* = (1 - k)^9. \quad (13)$$

Now the expression for the integral in the right-hand side of (10) can be derived explicitly and the dimensionless rebound threshold parameter B for turbulent flow can be expressed in the form

$$B = \frac{\delta \rho_{gas} U_{plate}^2 (1 - k)^{11}}{55 D_{drop} \rho_{drop} U_{d,n}^2}. \quad (14)$$

Expression for the threshold conditions for rebound (14) has been developed using the theory which neglects completely the surface tension effects. These effects can be taken into account by considering the aerodynamic Weber number

$$We_{aero} = \frac{\rho_{gas} D_{drop} U_{plate}^2}{\sigma} \quad (15)$$

In Fig. 5 the outcome map of drop impact onto a rotating disk is shown in terms of the B number and the Weber number We_{aero} for turbulent air flow.

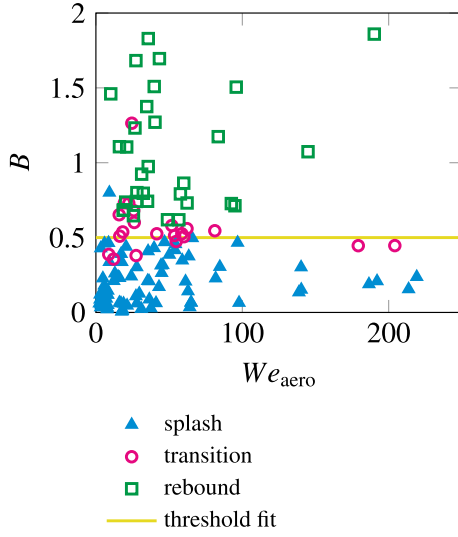


Fig. 5. Outcome map of drop impact onto a rotating disk in terms of the dimensionless parameter B , defined in (10), and We_{aero} , defined in (15). The experimental parameters correspond to the turbulent flow in the airflow around the disk.

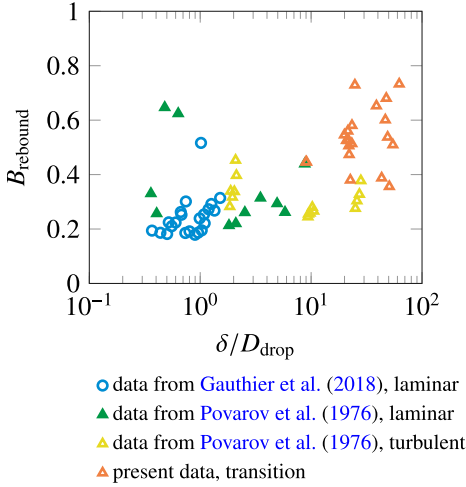


Fig. 6. Dependence of the rebound threshold parameter $B_{rebound}$ on the geometrical parameter δ/D_{drop} for the experimental data from Gauthier et al. (2018) with range of oil drop diameters $1.4 < D_{drop} < 3.1$ mm and from Povarov et al. (1976) with the range of water drop diameters $0.3 < D_{drop} < 4$ mm.

It becomes evident that $B_{rebound}$ is well suited to describe the onset of the aerodynamic rebound regime. Furthermore, a slight dependence of $B_{rebound}$ on We_{aero} becomes apparent at smaller values of the Weber number $We_{aero} < 10$. As expected, this dependence is minor at high values of We_{aero} for which

$$B_{rebound} \approx 0.5, \quad \text{for } We_{aero} > 10. \quad (16)$$

It is important to note that the fitted value of the parameter $B_{rebound}$ is of the order of unity. This is an important indicator of the validity of the model in which the main physical factors are taken into account.

At this stage the validity range of parameters of the solution for the deformation velocity (8) can be examined. The model used in this study is valid if the ratio of the steady and unsteady pressures, expressed in (5), satisfies the condition $p_{drop}/p_{drop,unsteady} \ll 1$. The upper bound for this ratio is estimated using (8):

$$\frac{p_{drop}}{p_{drop,unsteady}} \approx \frac{\delta^2}{D_{drop}^2} \frac{\rho_{gas} U_{plate}^2}{\rho_{drop} U_{drop}^2} \left[\int_0^1 f(\xi)^2 d\xi \right]^2. \quad (17)$$

In the example $U_{plate} = 140$ m/s, $U_{drop} = 1$ m/s, $D_{drop} = 0.56$, the estimation (17) yields $p_{drop}/p_{drop,unsteady} \approx 0.03$. The experimental parameters in this study satisfy the condition $p_{drop}/p_{drop,unsteady} \ll 1$; thus the assumptions in this model are justified.

3.4. Solution for laminar boundary layer, normal impact ($k = 0$)

In the case of a laminar boundary layer a similarity solution for the velocity distribution has been developed by von Kármán (1921) and solved by Cochran (1934). The boundary layer thickness, defined as the normal distance to the plate from a point where the air velocity has reached 1% of the plate velocity, is expressed (Schlichting and Gersten, 2016) in the form

$$\delta = 5.5 \sqrt{\nu_{gas}/\omega}, \quad (18)$$

where ω is the angular plate velocity, ν_{gas} is the gas kinematic viscosity.

The evolution of the air velocity can be obtained by numerically solving the coupled ordinary differential equation system from von Kármán (1921). Correspondingly, the three components of the gas velocity can be expressed in terms of the similarity variable $\xi = z/\delta$. The numerical integration of the expression on the right-hand side of (10), using the velocity profile $f(\xi)$ for laminar flow, yields

$$B = \frac{0.12 \delta \rho_{gas} U_{plate}^2}{D_{drop} \rho_{drop} U_{d,n}^2}, \quad \text{laminar flow, } k = 0. \quad (19)$$

The dependence of the rebound threshold parameter $B_{rebound}$, computed using Eq. (19), on the geometrical parameter δ/D_{drop} , as well as the values of $B_{rebound}$, computed with the help of (14), is shown in Fig. 6 using the experimental data from Gauthier et al. (2018) for silicon oil drops ($\nu = 100$ mm²/s, $\rho = 960$ kg/m³, $\sigma = 21$ mN/m) and from Povarov et al. (1976) for water.

Moreover, the results (Povarov et al., 1976) for $B_{rebound}$ in the turbulent regime are also in the same order of magnitude, indicating a clear improvement of the present model, which accounts for the velocity profile in the air boundary layer.

The scatter of the data for $B_{rebound}$ indicates that the parameter B is rather sensitive to the variations of the impact parameters. We can identify a monotonic but weak growth of $B_{rebound}$ for higher values of δ/D_{drop} . Nevertheless, the threshold values of B are in the range $0.18 < B_{rebound} < 0.8$.

4. Conclusion

In this study, drop impact onto a dry rotating plate is experimentally investigated using a high-speed video system. Various types of impact outcomes have been observed for water drops in the diameter range of $80 \mu\text{m} < D < 500 \mu\text{m}$ and relative tangential velocities of $40 \text{ m/s} < U_{\varphi,rel} < 160 \text{ m/s}$. These outcomes include drop complete or partial rebound, splash and deposition.

The threshold conditions for the drop full rebound are determined from experiments and are modeled theoretically. In the model, the drop deformation velocity caused by the aerodynamic pressure in the near-wall boundary layer of the airflow is estimated from the balance of the pressure at the drop surface. The corresponding dimensionless parameter B has been formulated, which is expressed not only in terms of the impact parameters and densities of liquid and gas but also on the entire velocity profile in the boundary layer. Since the inertial effects in the gas flow and deforming drop are dominant, the dependence of the threshold value of the parameter $B_{rebound}$, corresponding to the rebound threshold, on the aerodynamic Weber number, is rather weak. The threshold values of $B = B_{rebound}$ are rather close for laminar and turbulent flow regimes which indicates that the main physical factors are considered in the model. Furthermore, a weak dependence of $B_{rebound}$ on the geometrical parameter δ/D_{drop} is identified.

CRediT authorship contribution statement

Bastian Stumpf: Writing – review & editing, Writing – original draft, Visualization, Methodology, Investigation, Formal analysis, Data curation. **Samaneh Abdi Qezeljah:** Writing – review & editing, Writing – original draft, Visualization, Methodology, Investigation, Formal analysis, Data curation. **Reda Kamal:** Writing – review & editing, Writing – original draft, Visualization, Methodology, Investigation, Formal analysis, Data curation. **Fabien Dezitter:** Supervision, Funding acquisition. **Alessandro Martuffo:** Supervision, Conceptualization. **Ilia V. Roisman:** Writing – review & editing, Supervision, Funding acquisition, Formal analysis, Conceptualization. **Jeanette Hussong:** Writing – review & editing, Supervision, Funding acquisition, Formal analysis, Conceptualization.

Declaration of competing interest

The authors declare that they have no known competing financial interests or personal relationships that could have appeared to influence the work reported in this paper.

Acknowledgments

The work of Samaneh Abdi Qezeljah is partially supported by the joint DFG/WWF Collaborative Research Centre CREATOR (DFG: Project-ID 492661287/TRR 361; WWF: 10.55776/F90) at TU Darmstadt, TU Graz and JKU Linz. Furthermore, this research project is funded by the German Federal Ministry for Economic Affairs and Energy (BMWi) within the framework concept “LuFo VI”, subproject “NANNY”. This project has received funding from the European Union’s Horizon Europe research and innovation program under the Marie Skłodowska-Curie grant agreement No 101072551 (TRACES). The authors gratefully acknowledge the valuable preliminary work done by Dr.-Ing. Mark Gloerfeld and the assistance in the experiments of Osaid Ur Rahman Siddiqui.

Data availability

We have made the data and the videos available at the following link: <https://zenodo.org/doi/10.5281/zenodo.12684793>.

References

Agbaglah, G., Josserand, C., Zaleski, S., 2013. Longitudinal instability of a liquid rim. *Phys. Fluids* 25 (2), <http://dx.doi.org/10.1063/1.4789971>.

Alfredsson, P.H., Kato, K., Lingwood, R., 2023. Flows over rotating disks and cones. *Annu. Rev. Fluid Mech.* 56, 45–68. <http://dx.doi.org/10.1146/annurev-fluid-121021-043651>.

Almohammadi, H., Amirfazli, A., 2017. Understanding the drop impact on moving hydrophilic and hydrophobic surfaces. *Soft Matter* 13 (10), 2040–2053. <http://dx.doi.org/10.1039/c6sm02514e>.

Crespo del Arco, E., Serre, E., Bontoux, P., Launder, B.E., 2005. Stability, transition and turbulence in rotating cavities. In: *Instability of Flows*. WIT Press, pp. 141–195. <http://dx.doi.org/10.2495/1-85312-785-X/05>.

Brenn, G., Tropea, C., 1996. Monodisperse sprays for various purposes — Their production and characteristics. *Part. Part. Syst. Charact.* 13 (3), 179–185. <http://dx.doi.org/10.1002/ppsc.19960130303>.

Cao, Y., Chen, K., 2010. Helicopter icing. *Aeronaut. J.* 114 (1152), 83–90. <http://dx.doi.org/10.1017/S0001924000003559>.

Cao, Y., Tan, W., Wu, Z., 2018. Aircraft icing: An ongoing threat to aviation safety. *Aerosp. Sci. Technol.* 75, 353–385. <http://dx.doi.org/10.1016/j.ast.2017.12.028>.

Cao, Y., Wu, Z., Su, Y., Xu, Z., 2015. Aircraft flight characteristics in icing conditions. *Prog. Aerosp. Sci.* 74, 62–80. <http://dx.doi.org/10.1016/j.paerosci.2014.12.001>.

Cham, T.S., Head, M.R., 1969. Turbulent boundary-layer flow on a rotating disk. *J. Fluid Mech.* 37 (1), 129–147. <http://dx.doi.org/10.1017/S0022112069000450>.

Cochran, W.G., 1934. The flow due to a rotating disc. *Math. Proc. Cambridge Philos. Soc.* 30 (3), 365–375. <http://dx.doi.org/10.1017/S0305004100012561>.

de Ruiter, J., Lagraauw, R., van den Ende, D., Mugele, F., 2014. Wettability-independent bouncing on flat surfaces mediated by thin air films. *Nat. Phys.* 11 (1), 48–53. <http://dx.doi.org/10.1038/nphys3145>.

Gauthier, A., Bird, J.C., Clanet, C., Quéré, D., 2016. Aerodynamic Leidenfrost effect. *Phys. Rev. Fluids* 1 (8), 084002. <http://dx.doi.org/10.1103/PhysRevFluids.1.084002>, https://ui.adsabs.harvard.edu/link_gateway/2016PhRvF...1h4002G.

Gauthier, A., Bouillant, A., Clanet, C., Quéré, D., 2018. Aerodynamic repellency of impacting liquids. *Phys. Rev. Fluids* 3 (5), 054002. <http://dx.doi.org/10.1103/PhysRevFluids.3.054002>, https://ui.adsabs.harvard.edu/link_gateway/2018PhRvF...3e4002G.

Geppert, A.K., 2019. Experimental Investigation of Droplet Wall-Film Interaction of Binary Systems (Ph.D. thesis). Institute of Aerospace Thermodynamics, University of Stuttgart, Stuttgart, <http://dx.doi.org/10.18419/opus-10577>.

Itoh, M., Hasegawa, I., 1994. Turbulent boundary layer on a rotating disk in infinite quiescent fluid. *JSME Int. J. Ser. B* 37 (3), 449–456. <http://dx.doi.org/10.1299/jsmeb.37.449>.

Josserand, C., Thoroddsen, S.T., 2016. Drop impact on a solid surface. *Annu. Rev. Fluid Mech.* 48, 365–391. <http://dx.doi.org/10.1146/annurev-fluid-122414-034401>.

Kind, R., Potapczuk, M., Feo, A., Golia, C., Shah, A., 1998. Experimental and computational simulation of in-flight icing phenomena. *Prog. Aerosp. Sci.* 34 (5–6), 257–345. [http://dx.doi.org/10.1016/S0376-0421\(98\)80001-8](http://dx.doi.org/10.1016/S0376-0421(98)80001-8).

Kobayashi, R., 1994. Review: Laminar-to-turbulent transition of three-dimensional boundary layers on rotating bodies. *J. Fluids Eng.* 116 (2), 200–211. <http://dx.doi.org/10.1115/1.2910255>.

Lee, J.D., Harding, R., Palko, R.L., 1984. Documentation of Ice Shapes on the Main Rotor of a UH-1H Helicopter in Hover. Technical Report, NASA, URL <https://api.semanticscholar.org/CorpusID:107149015>.

Lim, D.H., Kim, S.C., 2014. Thermal performance of oil spray cooling system for in-wheel motor in electric vehicles. *Appl. Therm. Eng.* 63 (2), 577–587. <http://dx.doi.org/10.1016/j.applthermaleng.2013.11.057>.

Lingwood, R.J., Henrik Alfredsson, P., 2015. Instabilities of the von Kármán boundary layer. *Appl. Mech. Rev.* 67 (3), 030803. <http://dx.doi.org/10.1115/1.4029605>.

Littell, H.S., Eaton, J.K., 1994. Turbulence characteristics of the boundary layer on a rotating disk. *J. Fluid Mech.* 266, 175–207. <http://dx.doi.org/10.1017/S0022112094000972>.

Liu, C., Xu, Z., Gerada, D., Li, J., Gerada, C., Chong, Y.C., Popescu, M., Goss, J., Staton, D., Zhang, H., 2019. Experimental investigation on oil spray cooling with hairpin windings. *IEEE Trans. Ind. Electron.* 67 (9), 7343–7353. <http://dx.doi.org/10.1109/TIE.2019.2942563>.

Moghtadernejad, S., Jadidi, M., Johnson, Z., Stolpe, T., Hanson, J., 2021. Droplet impact dynamics on an aluminum spinning disk. *Phys. Fluids* 33 (7), <http://dx.doi.org/10.1063/5.0050997>.

Moreira, A., Moita, A.S., Panao, M.R., 2010. Advances and challenges in explaining fuel spray impingement: How much of single droplet impact research is useful? *Prog. Energy Combust. Sci.* 36, 554–580. <http://dx.doi.org/10.1016/j.pecs.2010.01.002>.

Mundo, C., Sommerfeld, M., Tropea, C., 1995. Droplet-wall collisions: Experimental studies of the deformation and breakup process. *Int. J. Multiph. Flow* 21 (2), 151–173. [http://dx.doi.org/10.1016/0301-9322\(94\)00069-V](http://dx.doi.org/10.1016/0301-9322(94)00069-V).

Povarov, O.A., Nazarov, O.I., Ignat'evskaya, L.A., Nikol'skii, A.I., 1976. Interaction of drops with boundary layer on rotating surface. *J. Eng. Phys.* 31 (6), 1453–1456. <http://dx.doi.org/10.1007/BF00860580>.

Riboux, G., Gordillo, J.M., 2014. Experiments of drops impacting a smooth solid surface: a model of the critical impact speed for drop splashing. *Phys. Rev. Lett.* 113 (2), 024507. <http://dx.doi.org/10.1103/PhysRevLett.113.024507>, https://ui.adsabs.harvard.edu/link_gateway/2014PhRvL.113b4507R.

Roisman, I.V., 2010. On the instability of a free viscous rim. *J. Fluid Mech.* 661, 206–228. <http://dx.doi.org/10.1017/S0022112010002910>.

Roisman, I.V., Lembach, A., Tropea, C., 2015. Drop splashing induced by target roughness and porosity: The size plays no role. *Adv. Colloid Interface Sci.* 222, 615–621. <http://dx.doi.org/10.1016/j.cis.2015.02.004>.

Roisman, I.V., Rioboo, R., Tropea, C., 2002. Normal impact of a liquid drop on a dry surface: model for spreading and receding. *Proc. R. Soc. Lond. Ser. A Math. Phys. Eng. Sci.* 458 (2022), 1411–1430. <http://dx.doi.org/10.1098/rspa.2001.0923>.

Roisman, I.V., Tropea, C., 2002. Impact of a drop onto a wetted wall: description of crown formation and propagation. *J. Fluid Mech.* 472, 373–397. <http://dx.doi.org/10.1017/S0022112002002434>.

Schlichting, H., Gersten, K., 2016. *Boundary-Layer Theory*. Springer London, Limited, <http://dx.doi.org/10.1007/978-3-662-52919-5>.

Shevchuk, I.V., 2009. Convective Heat and Mass Transfer in Rotating Disk Systems. Springer, p. 239. <http://dx.doi.org/10.1007/978-3-642-00718-7>.

Shevchuk, I.V., Khalatov, A.A., 1997. Integral method for calculating the characteristics of a turbulent boundary layer on a rotating disk: Quadratic approximation of the tangent of the flow swirl angle. *Heat Transfer Res.* 28 (4–6), 402–413. <http://dx.doi.org/10.1615/HeatTransRes.v28.i4-6.280>.

Sprittles, J.E., 2024. Gas microfilms in droplet dynamics: When do drops bounce? *Annu. Rev. Fluid Mech.* 56 (1), 91–118. <http://dx.doi.org/10.1146/annurev-fluid-121021-021121>.

Stumpf, B., Roisman, I.V., Yarin, A.L., Tropea, C., 2023. Drop impact onto a substrate wetted by another liquid: corona detachment from the wall film. *J. Fluid Mech.* 956, 625. <http://dx.doi.org/10.1017/jfm.2022.1060>.

Taylor, G.I., 1959. The dynamics of thin sheets of fluid II. Waves on fluid sheets. *Proc. R. Soc. Lond. Ser. A Math. Phys. Eng. Sci.* 253 (1274), 296–312. <http://dx.doi.org/10.1098/rspa.1959.0195>.

- Theodorsen, T., Regier, A., 1944. Experiments on drag of revolving disks, cylinders, and streamline rods at high speeds. NACA Techn. Rep. 793 (3), URL <http://hdl.handle.net/2060/20050241738>.
- Tropea, C., Marengo, M., 1999. The impact of drops on walls and films. *Multiphase Sci. Technol.* 11 (1), 19–36. <http://dx.doi.org/10.1615/MultScienTechn.v11.i1.20>.
- von Kármán, T.V., 1921. Über laminare und turbulente Reibung. *Z. Angew. Math. Mech.* 1 (4), 233–252. <http://dx.doi.org/10.1002/zamm.19210010401>, https://ui.adsabs.harvard.edu/link_gateway/1921ZaMM....1..233K.
- von Kármán, T., 1946. On Laminar and Turbulent Friction. National Advisory Committee on Aeronautics.
- Wang, Y., Bourouiba, L., 2021. Growth and breakup of ligaments in unsteady fragmentation. *J. Fluid Mech.* 910, A39. <http://dx.doi.org/10.1017/jfm.2020.698>.
- Xu, L., Zhang, W.W., Nagel, S.R., 2005. Drop splashing on a dry smooth surface. *Phys. Rev. Lett.* 94 (18), 184505. <http://dx.doi.org/10.1103/physrevlett.94.184505>.
- Yamazaki, M., Jemcov, A., Sakaue, H., 2021. A review on the current status of icing physics and mitigation in aviation. *Aerospace* 8 (7), 188. <http://dx.doi.org/10.3390/aerospace8070188>.
- Yarin, A.L., 2006. Drop impact dynamics: splashing, spreading, receding, bouncing. . . . *Annu. Rev. Fluid Mech.* 2006 (38), 159–192. <http://dx.doi.org/10.1146/annurev.fluid.38.050304.092144>.
- Yarin, A.L., Roisman, I.V., Tropea, C., 2017. *Collision Phenomena in Liquids and Solids*. Cambridge University Press, <http://dx.doi.org/10.1017/9781316556580>.
- Yarin, A.L., Weiss, D.A., 1995. Impact of drops on solid surfaces: self-similar capillary waves, and splashing as a new type of kinematic discontinuity. *J. Fluid Mech.* 283, 141–173. <http://dx.doi.org/10.1017/S0022112095002266>.
- Zhu, J., Tu, C., Lu, T., Luo, Y., Zhang, K., Chen, X., 2021. Behavior of a water droplet impacting a thin water film. *Exp. Fluids* 62, 143. <http://dx.doi.org/10.1007/s00348-021-03245-0>.